



1 **Fatigue life evaluation of offshore wind turbines considering**
2 **scour and passive structural control**

3
4 Yu Cao¹, Ningyu Wu², Jigang Yang², Chao Chen^{1,3*}, Ronghua Zhu^{3,4*}, Xugang Hua¹,
5

6 ¹Key Laboratory for Bridge and Wind Engineering of Hunan Province, College of Civil
7 Engineering, Hunan University, Changsha, China

8 ²Hebei Construction Investment Offshore Wind Power Co., Ltd., Tangshan, China

9 ³Yangjiang Offshore Wind Laboratory, Yangjiang, China

10 ⁴Ocean College, Zhejiang University, Hangzhou, China

11

12

13

14

15

*Corresponding author: steinchen@hnu.edu.cn, zhu.richard@zju.edu.cn



16 Abstract

17 Offshore wind turbine (OWT) support structures are exposed to the risk of fatigue
18 damages and scour, and this risk can be effectively mitigated by installing structural
19 control devices such as tuned mass dampers (TMDs). However, time-varying scour al-
20 tering OWTs' dynamic characteristics has an impact on the TMD design and fatigue
21 life, which was rarely studied before. In this paper, a simplified modal model was used
22 to investigate the influence of scour and a TMD on the fatigue life evaluation of a 5
23 MW OWT's support structure, and the parameters of the TMD were obtained by either
24 a traditional method or a newly developed optimization technique. This optimization
25 technique aims at finding optimal parameters of the TMD which maximizes the fatigue
26 life of a hotspot at the mudline, and effect of time-varying scour can be considered.
27 Results show that scour can decrease the fatigue life by about 26%, and the TMD can
28 effectively suppress vibration and increase the fatigue life. Further, it is found that the
29 fatigue life can be extended by 7.2% with the TMD optimized by the proposed opti-
30 mization technique, compared to that with the traditionally optimized TMD which does
31 not take the change of dynamic characteristics into account.

32 **Keywords:** scour, offshore wind turbine, structural control, modal analysis, fatigue life.

33

34 1 Introduction

35 With the continuous development of large-size fixed-bottom offshore wind tur-
36 bines, scour around pile foundations has become a common issue (Prendergast et al.,
37 2015; L. Wang et al., 2020; X. Wang et al., 2019), as scour can have a significant impact
38 on dynamic characteristics, vibration magnitudes, and thus fatigue life of OWTs under
39 wind and wave loads. The action of currents and waves causes local scour pits around
40 pile foundations, which reduces the burial depth of pile foundations. This phenomenon
41 usually causes a reduction in natural frequencies of OWTs and changes in other dy-
42 namic characteristics, possibly leading to resonance when one of natural frequencies is
43 close to the rotational frequency of the blades (Peder Hyldal Sørensen and Bo Ibsen,
44 2013). On the other hand, the harsh offshore environment causes OWTs' long-term
45 vibration and stress cycling in wind turbine components, endangering these compo-
46 nents' fatigue durability (Herbert and Paul, 1994). Fatigue has become the main cause
47 of wind turbine tower failure (Sørensen et al., 2008). Thus, the scour-induced changes



48 in dynamic characteristics and risk in resonance inevitably induce an increase in fatigue
49 damages and deserve in-depth research.

50 Many researchers have studied the effect of scouring on fatigue damage accumu-
51 lation in OWTs. For instance, Tempel et al. (2006) investigated the frequency and fa-
52 tigue of piles under different scour depths and concluded that scour has a little effect
53 on the natural frequencies but a great effect on fatigue damage. Zhang et al. (2021)
54 found that scour depth has a significant influence on monopile impedance. Rezaei et al.
55 (2018) showed that scour leads to an increase in the maximum bending moment of the
56 monopile and a shortening of the fatigue life. To mitigate the fatigue damages in OWTs,
57 installing structural control devices is an effective way. It was demonstrated that tuned
58 mass dampers (TMDs) have a positive effect on reducing vibration amplitudes of wind
59 turbine systems (Lackner and Rotea, 2011; Enevoldsen and Mørk, 1996; Dinh and Basu,
60 2015; Si et al., 2013). Dai et al. (2021) conducted a shaker experiment using a scaled
61 wind turbine model and showed that the installed TMD can suppress the vibration of
62 the structure more effectively considering soil-structure interaction (SSI).

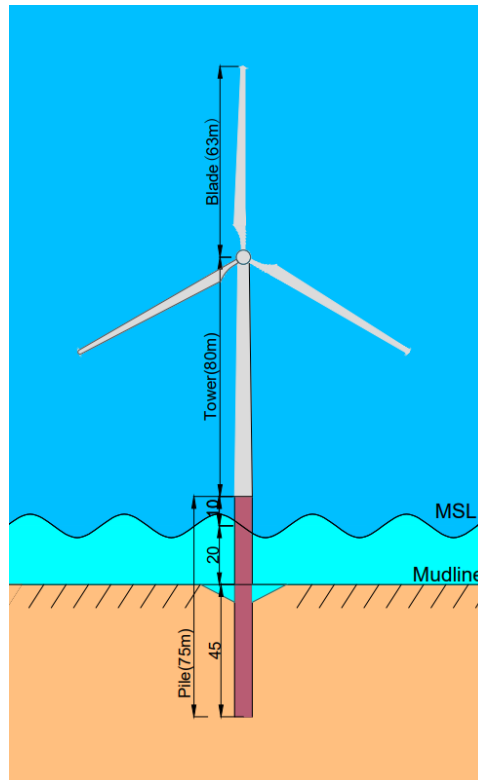
63 In the previously mentioned studies, researchers have individually investigated the
64 effect of scour on structural vibration and fatigue, and the structural control by TMDs
65 for OWTs. However, in practice, the effect of scour combining structural control via
66 TMDs could have a significant impact on OWTs' fatigue life. Moreover, whether con-
67 sidering scour could influence the design of TMDs, and TMDs with different parame-
68 ters can also have an impact on fatigue damage accumulation.

69 In this study, ABAQUS was used to establish a detailed SSI model with different
70 scour depths. A finite element (FE) model was created in MATLAB to consider scour
71 effect, wind loading and the TMD, then this FE model was simplified to a modal model
72 for the purposed of rapid fatigue life prediction by using a well-established method
73 previously presented by the authors. This study investigates the effect of different scour
74 depths on the performance of the TMD and the fatigue life of a 5 MW OWT's support
75 structure including a tower and a monopile foundation, and the optimization of the
76 TMD's parameters considering time-varying scour depths to maximum fatigue life was
77 also presented. This study can provide a guidance for the fatigue life evaluation and
78 TMD design for OWTs.



79 2 **Model description**

80 2.1 **Finite element model and implementation of tuned mass damper**



81

82 Fig. 1. Schematic of NREL 5MW wind turbine and scour effect

83 A FE model of an monopile-supported OWT installed with a TMD was established
84 in MATLAB. This model contains a flexible tower, a rotor-nacelle assembly (RNA),
85 and an external TMD, considering the foundation flexibility. The model is based on the
86 widely used NREL 5MW reference offshore wind turbine, and its detailed properties
87 are shown in Table 1. Three-dimensional beam elements are used to create the FE
88 model (C. Chen et al., 2023). The wind turbine tower is divided into 18 beam elements,
89 and the monopile between the mudline and the mean sea level (MSL) are divided into
90 4 beam elements. Each element node has 6 degrees of freedom (DOFs) corresponding
91 to the translational and rotational motions in different directions. The mass matrix and
92 stiffness matrix in the equation of motion of the OWT structure can be obtained given
93 the material properties. The damping matrix is applied by means of Rayleigh damping,



94 and the sum of soil damping and structural damping is assumed to be 1%. The RNA is
 95 represented by a lumped mass at the tower top.

96 The TMD is mounted on the top of the tower, and the effect of the TMD is con-
 97 sidered by adding its mass, damping, and stiffness terms at relevant positions in the
 98 local mass, damping, and stiffness matrices of the beam element representing the tower
 99 top. The equation of motion of the OWT main structure is:

$$\mathbf{M}_s \ddot{\mathbf{u}}_s + \mathbf{C}_s \dot{\mathbf{u}}_s + \mathbf{K}_s \mathbf{u}_s + \mathbf{C}_T(\dot{\mathbf{u}}_s - \dot{\mathbf{u}}_T) + \mathbf{K}_T(\mathbf{u}_s - \mathbf{u}_T) = \mathbf{F}_{\text{wind}} + \mathbf{F}_{\text{wave}}, \quad (1)$$

100 where \mathbf{M}_s , \mathbf{C}_s , \mathbf{K}_s are the mass, damping and stiffness matrices of the main structure.
 101 On the other hand, the equation of motion for the TMD can be represented by

$$\mathbf{m}_T \ddot{\mathbf{u}}_T + \mathbf{c}_T(\dot{\mathbf{u}}_T - \dot{\mathbf{u}}_s) + \mathbf{k}_T(\mathbf{u}_T - \mathbf{u}_s) = 0, \quad (2)$$

102 where \mathbf{m}_T , \mathbf{c}_T , \mathbf{k}_T are the mass, damping and stiffness of the TMD, \mathbf{u}_s is the displace-
 103 ment vector of the tower top, \mathbf{u}_T is the displacement vector of the TMD, and
 104 \mathbf{F}_{wind} , \mathbf{F}_{wave} are the aerodynamic and wave loads. The modelling of SSI is realized by
 105 an equivalent stiffness matrix, which will be introduced in detail subsequently in Sec-
 106 tions 2.3.

107 Table 1. Basic properties of the NREL 5MW reference OWT (J. Jonkman et al., 2009;
 108 Rezaei, 2017)

Number of blade	3
Rotor diameter	126 m
Tower length	80 m
Tower diameter	3.87–6.00 m
Tower thickness	28–38 mm
Pile length	65 m
Pile penetration depth	45 m
Pile diameter	6 m
Pile thickness	80 mm
Hub height from MSL	92.4 m
Turbine mass	350000 kg
Blade mass	17740 kg
Rated wind Speed	12.1 m/s



109 Wind loads were calculated using modified unsteady blade element momentum
110 (BEM) theory (Branlard, 2017; B. J. Jonkman and Buhl, 2006) with Prandtl and Glauert
111 corrections. Ignoring the iterative loop (C. Chen, Duffour, Fromme, et al., 2021a) in the
112 steady-state BEM code, the instantaneous aerodynamic forces were calculated for each
113 time step within the time integration. The turbulent wind field was generated using the
114 Kaimal spectrum according to the wind field parameters of IEC 61400-3 (2019) as-
115 suming moderate turbulence intensity. It should be noted that the aerodynamic loads
116 from the rotor applied at the tower top were calculated using an aerodynamic force
117 linearization technique previously developed by the authors (C. Chen, Duffour,
118 Fromme, et al., 2021b; C. Chen et al., 2020). This technique divides the aerodynamic
119 loads into two parts. The first part is the quasi-steady aerodynamic force calculated by
120 BEM theory, which does not consider the influence of tower top motion. The second
121 part considers the effect of aerodynamic damping by introducing an additional aerody-
122 namic damping matrix. The adoption of this technique is to enable the development of
123 the simplified modal model for rapid fatigue calculation, which will be introduced in
124 detail in Subsection 2.4. Wave loads were calculated using the Morison equation, which
125 includes viscous drag and inertial forces:

$$\mathbf{F}_{\text{wave}} = \frac{1}{2} \rho_w D_{\text{pile}} C_d |\dot{\mathbf{u}}_w| \dot{\mathbf{u}}_w + \frac{\pi}{4} \rho_w D_{\text{pile}}^2 C_m \ddot{\mathbf{u}}_w, \quad (3)$$

126 where $\dot{\mathbf{u}}_w$ and $\ddot{\mathbf{u}}_w$ are the velocity and acceleration of water particles, C_d is the drag
127 coefficient, D_{pile} is the diameter of the monopile between the mean sea level and the
128 mudline, C_m is the inertia coefficient and ρ_w is the density of water. C_d and C_m were
129 chosen as 1 and 2 respectively as the recommended values in Ref. (Shirzadeh et al.,
130 2013). The wave profiles were obtained through the superposition of wave components,
131 combining linear wave theory and JONSWAP spectra (Klaus et al., 1973).

132 2.2 Scour modelling in ABAQUS

133 Using solid elements to model pile-soil interaction (C. Chen and Duffour, 2018;
134 S. Dai et al., 2021; Fard et al., 2022; Ma and Chen, 2021; Zdravković et al., 2015) is
135 usually considered to be more accurate than the p-y curve method (Liang et al., 2018;
136 Tempel, 2006) and the equivalent embedding method (Shahmohammadi and Sha-
137 bakhty, 2020; Bergua et al., 2022). The solid element method can also reduce the influ-
138 ence of empirical formula on the results. Therefore, the solid element method was used



139 to establish the wind turbine scour model. The wind turbine scour model established in
140 ABAQUS contains soil, pile foundation, tower, and the RNA is replaced by a concen-
141 trated mass located at the top of the tower. The diameter of the soil body is selected as
142 20 times of the pile diameter, the soil under the pile foundation is selected as 2.5 times
143 of the pile diameter, and the total height of the soil body is 60 m. The soil body is made
144 of homogeneous dense sandy soil, and the piles and tower are made of steel. The mate-
145 rial parameters of the soil body, pile and tower are shown in Table 2 below:

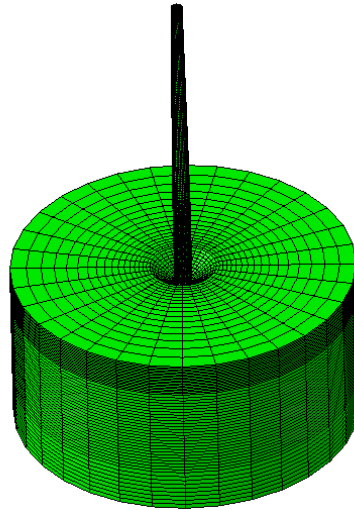
146 Table 2. Soil, pile and tower material parameters

Type	Weight γ (kN/m ³)	modulus of elasticity E_s (MPa)	Poisson's ratio ν	Internal friction angle φ (°)	Expansion angle ψ (°)	Cohesion c (kPa)
Soil	19	80	0.3	35	23	0.1
Pile	78.5	215	0.25	-	-	-
Tower	85	215	0.25	-	-	-

147 The Mohr-Coulomb model is used for the soil, and the pile, tower, and nacelle are
148 assumed to be elastic as they are much stiffer than the soil and do not deform plastically
149 for the normal operational conditions. The pile and tower are connected by a binding
150 relationship. The normal contact between the pile and soil adopts the hard contact, and
151 the tangential contact adopts the friction penalty function. The relative sliding friction
152 factor at the interface, μ is equal to $\tan(0.75 \varphi)$, where φ is the internal friction angle.
153 The pile-soil contact is in the form of frictional contact, where mutual contact pairs are
154 established between the pile and the soil, including the contacts between the pile bottom
155 surface and the soil, between the outside surface of the pile and the soil, and the inside
156 surface of the pile and the soil core. The frictional contact between pile bottom surface
157 and soil is omitted due to the small area of the contact surface. These frictional contacts
158 all adopt the face-to-face contact, and the contact discretization method adopts the face-
159 to-face discretization method, considering the large stiffness of the main surface and
160 small stiffness of the slave surface. The perimeter of the soil body is translationally
161 constrained, and the bottom surface of the soil adopts a fixed constraint. The eight-node
162 linear brick element (C3D8R) was used to model the pile and soil, and the mesh division
163 is realized by arranging seeds as shown in Fig. 2. The whole model was set up by adopt-
164 ing the modelling method of “element birth and death”, which realizes the operation of



165 initial soil stress balance and sets up contacts and other related steps by killing and
166 activating relevant elements.



167

168 Fig. 2. Pile-soil interaction modelled by ABAQUS

169 The scour conditions can be represented by a deep conical pit around the pile under
170 the long-term action of the waves and currents. According to the specification of Det
171 Norske Veritas (DNV) (2014b), the radius of the pit surface formed by scour, R, can
172 be related to the depth of the scour pit by

$$R = \frac{D}{2} + \frac{S}{\tan\varphi}, \quad (4)$$

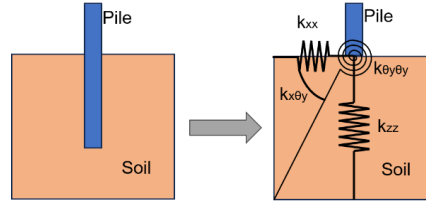
173 where D is the diameter of the pile, S is the scour depth, and φ is the angle of internal
174 friction of the soil.

175 2.3 Equivalent stiffness matrix method

176 It is necessary to consider the effect of scour in the FE model in MATLAB. An
177 equivalent stiffness matrix method was adopted in the FE model to consider the flexi-
178 bility induced by SSI. The 6 DOFs of node at the mudline are assumed to be constrained
179 by a series of coupled springs, and the stiffnesses of the coupled springs form a 6×6
180 stiffness matrix. For one specific stiffness term used in the FE model, for instance the
181 one relevant to the lateral displacement in the fore-aft (FA) direction, the value of the
182 stiffness term can be found from the relationship between the reaction force at the



183 mudline and the pile top displacement (Jung et al., 2015). The equivalent stiffness sche-
 184 matic of the pile-soil interaction in the FA direction for the OWT is shown in Fig. 3.



185

186 Fig. 3. Equivalent stiffness schematic of pile-soil interaction in the FA direction

187 According to the principle of virtual displacement and with the DOFs in the other
 188 directions constrained, a unit displacement or rotation was first applied in one direction,
 189 and then the reaction force in that direction can be known. The equivalent stiffness in
 190 that direction can be subsequently calculated by the relationship between the displace-
 191 ment and reaction force. Using the same approach, the stiffness terms corresponding to
 192 the remaining five DOFs were calculated. The stiffness terms in all the six DOFs to-
 193 gether form all the diagonal terms of the soil stiffness matrix. With the diagonal terms
 194 known, the off-diagonal stiffness terms can be found by applying a unit displacement
 195 in one direction and looking at the reaction force in the other concerned direction,
 196 with the other four DOFs constrained. Using the same principle, the off-diagonal terms can
 197 also be found from the relationship between the displacements and reaction forces,
 198 which ultimately results in a 6×6 stiffness matrix (Bergua et al., 2021; Pedersen and
 199 Askheim, 2021):

$$\mathbf{F}_{\text{soil}} = \begin{Bmatrix} F_x(t) \\ F_y(t) \\ F_z(t) \\ M_x(t) \\ M_y(t) \\ M_z(t) \end{Bmatrix} = \begin{bmatrix} k_{xx} & 0 & 0 & 0 & k_{x\theta_y} & 0 \\ 0 & k_{yy} & 0 & k_{y\theta_x} & 0 & 0 \\ 0 & 0 & k_{zz} & 0 & 0 & 0 \\ 0 & k_{\theta_{xy}} & 0 & k_{\theta_x\theta_x} & 0 & 0 \\ k_{\theta_{yx}} & 0 & 0 & 0 & k_{\theta_y\theta_y} & 0 \\ 0 & 0 & 0 & 0 & 0 & k_{\theta_z\theta_z} \end{bmatrix} \begin{Bmatrix} u_x(t) \\ u_y(t) \\ u_z(t) \\ \theta_x(t) \\ \theta_y(t) \\ \theta_z(t) \end{Bmatrix} \quad (5)$$

$$= \mathbf{K}_{\text{soil}} \mathbf{u}_{\text{soil}} .$$

200 where \mathbf{K}_{soil} is the equivalent soil stiffness matrix, \mathbf{u}_{soil} is the displacement vector, and
 201 \mathbf{F}_{soil} is the reaction force vector. The 6×6 soil stiffness matrix obtained from ABAQUS
 202 is imported to the FE model in MATLAB. This modelling method possesses the ad-
 203 vantages of the increase in accuracy brought by the scour model in ABAQUS with solid



204 elements, and the fast calculation speed and convenience in applying wind and wave
205 loads brought by the usage of the FE model in MATLAB.

206

207 2.4 Rapid fatigue evaluation method

208 The established FE model in MATLAB can generate dynamic responses of the
209 OWT, considering wind and wave loads and scour effect. However, a comprehensive
210 fatigue life prediction in time domain needs to consider a large number of environmen-
211 tal states and load cases, so simulation efficiency is very important. Moreover, the
212 TMD design optimization requires much more dynamic response time series. The FE
213 model is not fast enough in this case. Therefore, a simplified modal model was devel-
214 oped from the FE model in MATLAB following the method develop in Ref. (C .Chen
215 et al., 2021). Since the dynamic responses of the OWT are mainly dominated by the
216 first two bending vibration modes, the FE model is reduced into a 4-DOF simplified
217 modal model by considering only the first two bending modes in the FA and side-side
218 (SS) directions respectively. The development of the simplified 4-DOF modal model is
219 briefly introduced as follows. Denoting the mass matrix and stiffness matrix of the
220 OWT as \mathbf{M} and \mathbf{K} including the TMD and the lumped soil stiffness matrix, the un-
221 damped vibration mode matrix Ψ can be obtained directly through eigen analysis. Mul-
222 tiplying the transpose Ψ^T of the undamped vibration matrix Ψ with the equation of mo-
223 tion the OWT, leading to the following equation:

$$\Psi^T \mathbf{M} \Psi \ddot{\mathbf{u}} + \Psi^T \mathbf{C} \Psi \dot{\mathbf{u}} + \Psi^T \mathbf{K} \Psi \mathbf{u} = \Psi^T \mathbf{F}. \quad (6)$$

224 Then rewrite the above equation as

$$\bar{\mathbf{M}} \ddot{\boldsymbol{\alpha}} + \bar{\mathbf{C}} \dot{\boldsymbol{\alpha}} + \bar{\mathbf{K}} \boldsymbol{\alpha} = \bar{\mathbf{F}}, \quad (7)$$

225 where $\boldsymbol{\alpha}$ is the general coordinate vector, $\bar{\mathbf{M}}$ is the modal mass matrix, $\bar{\mathbf{C}}$ is the modal
226 damping matrix, $\bar{\mathbf{K}}$ is the modal stiffness matrix, $\bar{\mathbf{F}}$ the modal load matrix. Truncating
227 the Eq. (6) by only considering the first two bending modes, the FE model is reduced
228 to a 4-DOF modal model, which can be used for a rapid fatigue analysis. The dynamic
229 responses of the OWT can be obtained by modal superposition which can be repre-
230 sented by the relationship $\mathbf{u} = \Psi \boldsymbol{\alpha}$, after solving the general coordinate vector by time
231 integration. In the 4-DOF simplified modal model, the cross-section stress at any height



232 can be calculated from the calculated node displacements. According to the dynamic
 233 stress extraction method provided by Pelayo et al. (2015), the cross-section stress $\sigma_z(t)$
 234 at any moment at a given location can be obtained by:

$$\sigma_z(t) = -E(\mathbf{N}^{e''}(z)\mathbf{u}_x^e(t) + \mathbf{N}^{e''}(z)\mathbf{u}_y^e(t)y), \quad (8)$$

235 where \mathbf{u}^e is the nodal displacement vector at the cross section, E is the material elastic
 236 modulus, and \mathbf{N}^e is the elemental shape function vector. After cyclic counting the stress
 237 time series using the rainfall counting method, the fatigue damage at the hotspot can be
 238 evaluated by utilizing the Palmgren-Miner rule based on the S-N fatigue calculation
 239 method. The S-N curve for steel under water can be obtained by the following equation
 240 considering the thickness effect in DNV (2014a):

$$\log N = \log \bar{a} - m \cdot \log \left[\Delta \sigma \left(\frac{t}{t_{ref}} \right)^k \right], \quad (9)$$

241 where N is the number of cycles to failure, $\Delta \sigma$ is the stress range, m is the negative in-
 242 verse slope of the S-N curve, and $\log \bar{a}$ is the intercept between the $\log N$ axis and the
 243 S-N curve, t_{ref} is the reference thickness for welded joints, t is the thickness at which
 244 cracks may grow and k is the thickness exponent of fatigue strength. For pile joints,
 245 $t_{ref} = 25\text{mm}$. According to the DNV code, a bilinear S-N curve is usually used for
 246 offshore structures subjected mainly to typical wind and wave loads, using the Class E
 247 structural detail S-N curve shown in Table 3.

248 Table 3 Class E structural detail S-N curves

$N \leq 10^6$		$N \geq 10^6$			t (mm)	SCF
m_1	$\log \bar{a}_1$	m_2	$\log \bar{a}_2$	k		
3.0	11.610	5.0	15.350	0.2	80	1.13

249 For variable amplitude stresses, the fatigue damage index is calculated using the
 250 Palmgren-Miner summation rule:

$$D_k = \sum_{i=1}^{N_c} \frac{n_i}{N_i}, \quad (10)$$

251 where N_c is the total number of bins obtained by rainflow counting, n_i is the number of
 252 cycles in stress range i , N_i is the number of cycles to failure in stress range i , and D_k is

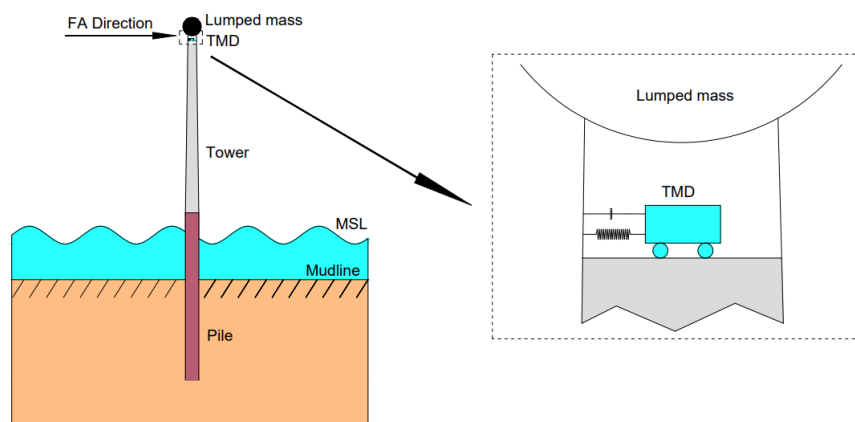


253 the total fatigue damage index. Fatigue failure occurs at the hotspot when the fatigue
254 damage index reaches one.

255 3 Damper design and optimisation method

256 Installing damping devices can efficiently reduce the vibration amplitudes of
257 OWTs so that their service life can be greatly prolonged. Using TMDs as passive control
258 devices is most widely used to control the vibration of OWT support structures.
259 Usually, most of TMDs are designed according to the dynamic characteristics of the
260 OWTs determined in the preliminary design stage, without considering the changes in
261 dynamic properties possibly caused by scour and soil degradation. However, in the real
262 environment, scour can cause the dynamic characteristics of OWTs to change, which
263 perhaps makes installed dampers become less effective or even completely ineffective.
264 Therefore, it is of great significance to consider the change in dynamic properties
265 caused by scour on the TMD design. The following two subsections first introduce the
266 traditional TMD design method considering constant dynamic characteristic in the initial
267 state, and then an optimal parameter searching method for the design of TMDs is
268 presented considering the effect of scour and fatigue life evaluation.

269 3.1 TMD design in initial state



270

271 Fig. 4. Schematic diagram of TMD arrangement in the tower tube

272 As the dominant vibration mode of the OWT structure in operation is the first
273 bending mode in the FA direction, the largest vibration amplitude occurs at the tower
274 top and installing the TMD at the tower top is most effective. Therefore, the TMD is



275 installed inside the steel tube at the tower top to mainly control the vibration in the FA
276 direction, as shown in Fig. 4. Accordingly, the initial design of the TMD is mainly
277 carried out based on the dynamic properties for the first-order mode. The initial design
278 is conduct based on the assumption that the monopile foundation is not scoured.

279 Numerous studies have shown that a TMD can effectively suppress the vibration
280 of a main structure when the mass ratio of the TMDs to the main structure is 1%-2%
281 (Y. Chen et al., 2021; R. Zhang et al., 2019). After determining the mass ratio of the
282 TMD to the OWT structure, according to the classic TMD optimization theory pro-
283 posed by Den Hartog (Den Hartog, 1957), the optimal frequency ratio of the TMD to
284 the OWT structure is

$$\alpha_{\text{opt}} = \frac{1}{1 + \mu}. \quad (6)$$

285 The optimal damping ratio for the TMD can be calculated by

$$\xi_{\text{opt}} = \sqrt{\frac{3\mu}{8(1 + \mu)}}, \quad (7)$$

286 where μ is the mass ratio of the TMD to the OWT structure, α_{opt} is the optimal fre-
287 quency ratio of the TMD to the OWT structure and is the optimal damping ratio of the
288 TMD.

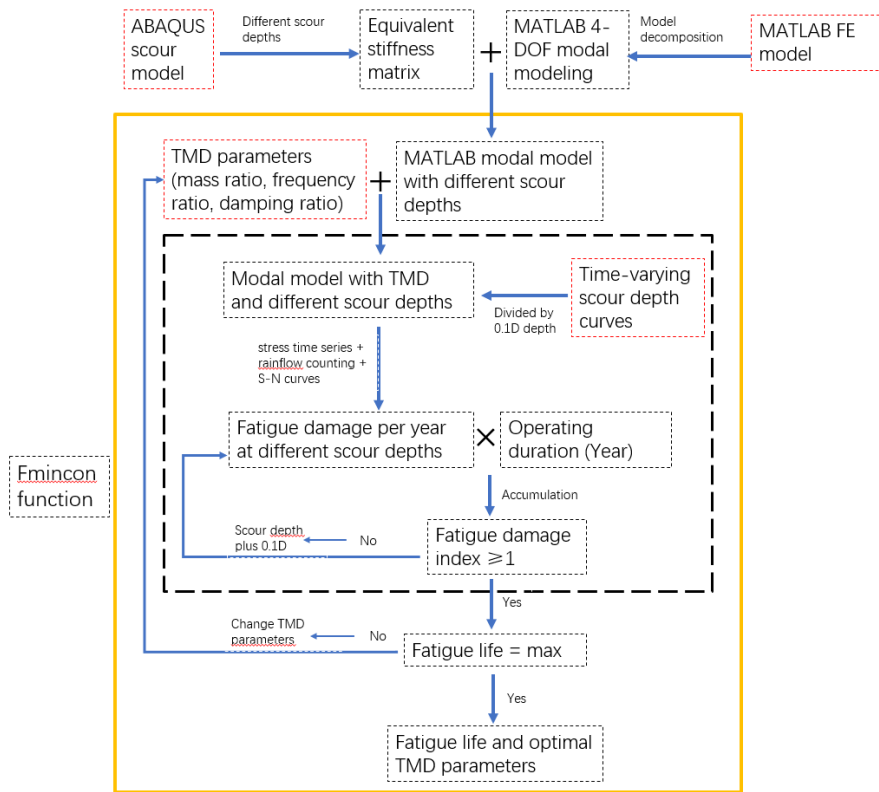
289 In this study, the mass ratio of the TMD system to the main structure was first
290 selected to be 1%. According to Den Hartog's optimization theory for the initial TMD
291 design, it can be determined that the optimal frequency ratio of the TMD to the main
292 structure is 0.99, and the optimal damping ratio of the TMD is 0.061. When the OWT
293 support structure is not scoured, the first-order modal mass of the structure is 440350
294 kg, and the first-order modal frequency is 0.265 Hz. Therefore, according to the initial
295 design parameters, the mass, stiffness coefficient and damping coefficient of the TMD
296 system are 4403.5 kg, 11,952 N/m and 885 N·s/m respectively.

297 3.2 Fatigue-based damper optimisation technique

298 After scour occurs around the monopile foundation, the burial depth of the mono-
299 pile and natural frequencies of the OWT gradually change. The vibration mitigation
300 effect of the TMD designed based on the dynamic parameters in the initial state can be



301 reduced, which may lead to the increase of fatigue damages of the OWT support struc-
 302 ture. Therefore, when designing the TMD, considering the influence of the time-vary-
 303 ing scour could enhance the performance of the TMD and thus result in a longer fatigue
 304 life of the support structure.



305

306 Fig. 6. Flowchart of TMD fatigue-life-based optimization technique

307 Here a fatigue-life-based optimization technique (FOT) to find optimal parameters
 308 of the TMD was developed in MATLAB as shown in Fig. 6. In this technique, the
 309 frequency ratio, mass ratio and damping ratio of the TMD were set as the optimal pa-
 310 rameters to search, and the fatigue life is the optimization objective. The simplified 4-
 311 DOF modal model incorporating scour modelling was used to generate the stress time
 312 series. The optimization problem is formed so that the optimal parameters of the TMD
 313 correspond to the longest fatigue life of the OWT support structure. The Fmincon func-
 314 tion in MATLAB was used to solve the optimization problem.



315 **4 Results**

316 **4.1 Environmental states and load cases**

317 In this study, fatigue analyses were performed under 22 environmental states pro-
 318 vided by Tempel (2006), taking into account both operational and parked situations.
 319 These 22 environmental states are shown in Table 4. The wind and wave loads are
 320 assumed to be always in the same direction to simplify the analysis. When the mean
 321 wind speeds are above the cut-in wind speed and below the cut-out wind speed, a 95%
 322 wind turbine availability is assumed following the setting in Ref. (Velarde et al., 2020),
 323 meaning that the OWT does not produce power for 5% when the mean wind speeds are
 324 in the operating range.

325 Table 4. Environmental states, adopted from Tempel (2006).

State	Vw (m/s)	Tz (s)	Hs (m)	P _{State} (%)	State	Vw (m/s)	Tz (s)	Hs (m)	P _{State} (%)
1	4	3	0.5	3.95	12	14	5	2	3.26
2	4	4	0.5	3.21	13	16	4	2	1.79
3	6	3	0.5	11.17	14	16	5	2.5	3.1
4	6	4	0.5	7.22	15	18	5	2.5	1.74
5	8	3	0.5	11.45	16	18	5	3	0.8
6	8	4	1	8.68	17	20	5	2.5	0.43
7	10	3	0.5	5.31	18	20	5	3	1.14
8	10	4	1	11.33	19	22	5	3	0.4
9	12	4	1	5.86	20	22	6	4	0.29
10	12	4	1.5	6	21	24	5	3.5	0.15
11	14	4	1.5	4.48	22	24	6	4	0.1

326 To investigate the effect of scouring and installation of the TMD on the fatigue damage
 327 accumulation, six load cases (LCs) were selected as shown in Table 5. LC 1 is used as
 328 the reference case, and other cases are distinguished by different scour and TMD set-
 329 tings. For LC 4 to LC 6, the initial design of the TMD with the mass ratio of 1% is
 330 used.

331 Table 5. Load case definition

LC number	TMD condition	Scour condition	LC number	TMD condition	Scour condition
LC 1	No	No Scour	LC 4	Enable	No Scour
LC 2	No	Time-varying	LC 5	Enable	Time-varying
LC 3	No	Maximum	LC 6	Enable	Maximum



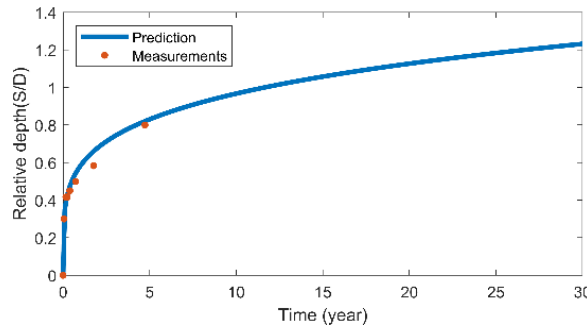
332 When considering the time-varying scour depth, for a particular time t , the time-varying
 333 scour depth S can be predicted by the equation provided by Nakagawa et al. (1976) was
 334 used:

$$S = \left(\frac{t}{t_1}\right)^{0.22} D. \quad (8)$$

335 where D is the diameter of the monopile, t_1 is the reference time and can be calculated
 336 by

$$t_1 = 29.2 \cdot \frac{D}{\sqrt{2} \cdot u} \cdot \left(\frac{\sqrt{\Delta \cdot g \cdot d_{50}}}{\sqrt{2} \cdot u - u_c}\right)^3 \cdot \left(\frac{D}{d_{50}}\right)^{1.9}. \quad (9)$$

337 u is the tidal velocity and taken as 0.5 m/s, u_c is the critical shear velocity and taken as
 338 0.37 m/s, g is the acceleration of gravity, d_{50} is grain size of sea sand. The parameter
 339 $\Delta = \frac{\rho_s}{\rho_w} - 1$, where ρ_s is density of sand, ρ_w is density of water. Rudolph et al. (2016)
 340 provided the sea state and measured the scour depths for the North Sea where the mono-
 341 pile N7 is located. The measured scour depth was fitted well for the first five years
 342 based on the time-varying scour depth prediction equation shown in Eq. (8). Therefore,
 343 the data from the North Sea site can represent a typical ocean environment with time-
 344 varying scour and was used for the correlation analysis in this study.



345
 346 Fig. 5. Time-varying scour depth curve for pile N7 in the North Sea

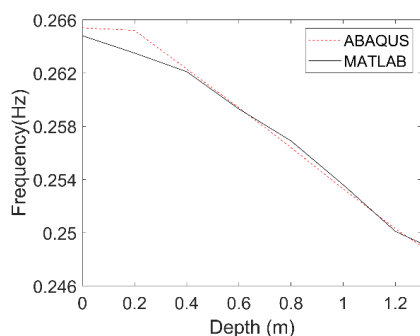
347 When conducting analysis with the time-varying scour, an increment of scour
 348 depth equal to 0.1D was used. At one particular scour depth, the fatigue damages were
 349 calculated and then the total fatigue damages during a longer period with a changing
 350 scour depth can be obtained by damage accumulation. According to the specification



351 of DNV, the maximum depth of a local scour pit formed around a pile foundation is 1.3
352 times the diameter of the pile. Therefore, it is assumed that the local scour pit has a
353 maximum scour depth of 1.3D at which the scour process achieves equilibrium.

354 4.2 Scour influence on natural frequencies

355 The scouring of the soil around the monopile has an important effect on the natural
356 frequencies of the OWT. For different scour depth, the first natural frequencies obtained
357 the by the models in ABAQUS and MATLAB are compared in Fig. 6. It shows the
358 increase in the scour depth leads to a decrease in the first natural frequency of the OWT.
359 The first natural frequency is 0.265 Hz when no scour occurs, and the natural frequency
360 is reduced to 0.248 Hz when the depth of the scour pit reaches the maximum depth. The
361 first natural frequency is reduced by 6.18% due to the maximum scour depth. It shows
362 that the natural frequency nearly monotonically decreases with the increase of the scour
363 depth. The installation of TMD also influences the natural frequency of the OWT main
364 structure. The TMD with a mass ratio of 1% makes the first natural frequency of the
365 OWT main structure reduces to 0.251 Hz when no scouring occurs, meaning that the
366 natural frequency is reduced by 5.4%.



367

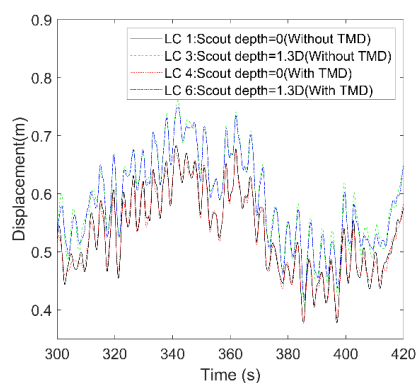
368 Fig. 6. Relationship between wind turbine natural frequency and scour depth

369 4.3 Dynamic response analysis

370 When the OWT is under the 9th environmental state which corresponds to the
371 rated wind speed of 12 m/s, a comparison for the tower top displacements is made for
372 LC 1, LC 3, LC 4 and LC 6, as shown in Fig. 7. These displacements are obtained from
373 the FE model in MATLAB described in Subsection 2.1. By comparing the displace-
374 ments from 300 seconds to 420 seconds for LC 1 and LC 4, it can be found that the
375 displacement amplitudes of the tower top decreases slightly by about 7% when the



376 TMD is installed. It is known that the aerodynamic damping is large when the OWT is
377 operating under the rated wind speed, so it is normal that the vibration mitigation effect
378 of the TMD is less significant in this case. The effect of the TMD is more prominent
379 for other operating conditions with less aerodynamic damping. Moreover, by compar-
380 ing the displacement responses for LC 1 and LC 3, it can be found that the average of
381 the displacement at the tower top increases by about 8% when the scour depth reaches
382 1.3D. This is because scour makes the OWT support structure become more flexible.



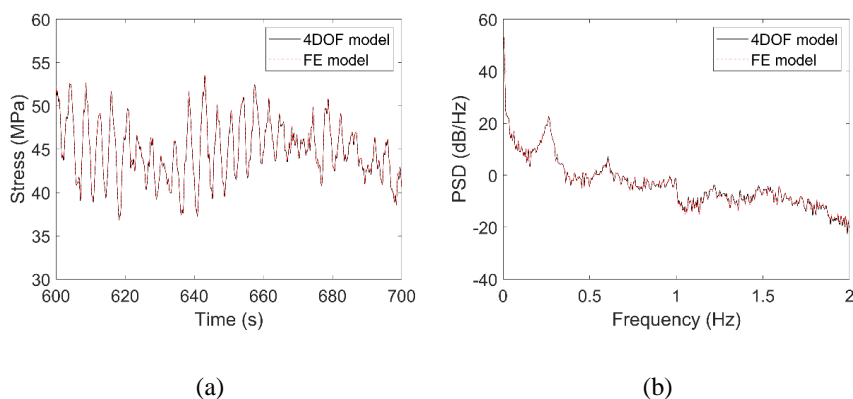
383

384 Fig. 7. Dynamic response of wind turbine under wind-wave coupled loads for four op-
385 erating conditions

386 4.4 Fatigue calculation results

387 In Subsection 2.4, it is mentioned that in the process of fatigue life analysis, the 4-
388 DOF simplified modal model was used to greatly save the calculation time. The accu-
389 racy test of the 4-DOF modal model in generating dynamic responses is first present in
390 this subsection. Under the turbulent wind field with a turbulence intensity of 11.9% and
391 an average wind speed of 12 m/s, the FE model and the 4-DOF simplified modal model
392 were used to calculate the stress responses at the mudline for 10 minutes.

393 As shown in Fig. 8, the stress responses from these two models are very close,
394 confirming good accuracy of the 4-DOF modal model. Moreover, the calculation time
395 of the 4-DOF simplified modal model is only about 1/55 of that of the FE model, which
396 shows that the 4-DOF simplified modal model is adequate to replace the FE model
397 when conducting fatigue life prediction.



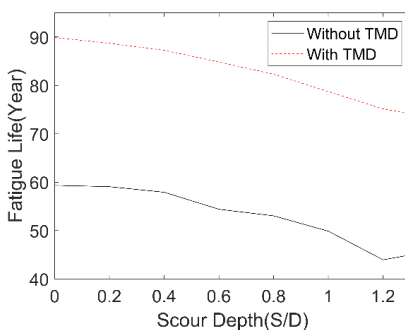
398 Fig. 8. Comparison of stresses at the mudline from the FE model and the 4-DOF
399 model in time domain (a) and frequency domain (b)

400 The 4-DOF simplified modal model was used to conduct fatigue life prediction for
401 the OWT support structure under LC 1 to LC 6. For a particular set of mean wind speed,
402 wave period and wave height, six different random seed numbers were used to generate
403 different wind fields and wave profiles to reduce the influence of randomness. A 10
404 min simulation for each random seed was conducted to obtain the stress time histories
405 at the mudline. The location of the hotspot used to evaluate fatigue damage is selected
406 at the point where maximum tensile stress reaches, and this point is in the support struc-
407 ture cross section at the mudline. Although the location in the monopile where the mo-
408 ment reaches its maximum value can be below the mudline, the location at the mudline
409 was picked for simplicity. Further, as the SSI is modelled in the FE model by an equiv-
410 alent soil stiffness matrix, it is unstraightforward to obtain the internal forces at the
411 cross sections below the mudline. Given the stress time series at the selected hotspot,
412 the corresponding fatigue damage was calculated. Then the fatigue damage for the set
413 of mean wind speed, wave period and wave height in 10 min was obtained by averaging
414 the fatigue damages for all the six random seeds. For all the 22 environment states, the
415 10 min fatigue damages were calculated, and the fatigue life was predicted according
416 to Palmgren-Miner sum rule by combing these calculated fatigue damages and the oc-
417 currence probabilities of the environmental states.

418 For different scour depths, the fatigue life of the OWT considering both operating
419 and parked conditions was predicted with or without TMD installation, and the results
420 are shown in Fig. 9. It is shown that an increase in scour depth leads to a decrease in



421 fatigue life, and an increasing fatigue life reduction rate can be observed when the scour
422 depth increases. When no scour occurs and the TMD is not installed on the OWT, the
423 OWT's fatigue life is 59.3 years, and the fatigue life drops to 45.0 years when consid-
424 ering the maximum scour depth of 1.3 D. There exist some uncertainties in the fatigue
425 life prediction process due to the generation of random wind field and wave profile. It
426 should be noted that the predicted fatigue life is much longer than the normally adopted
427 OWTs' design fatigue life of 25-30 years. This can be explained by the following rea-
428 sons. First, the maximum moment of the OWT support structure is not at the cross
429 section at the mudline where the selected hotspot is located. Second, the complex wind
430 and wave directionality during the OWT's lifetime is simplified, which would influence
431 the fatigue calculation result. Third, many other operation conditions such as starting
432 up, shutting down phases are not considered in this study, which can also have an im-
433 pact on the fatigue damage accumulation. Moreover, the installation of the TMD greatly
434 extends about 50% of the OWT support structure's fatigue life.



435

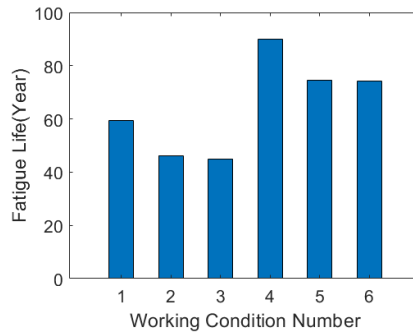
436 Fig. 9. Frequency life of wind turbine with different scour depths

437 The fatigue life prediction results of the OWT were obtained for all the six LCs,
438 as shown in Fig. 10. The fatigue life from the reference case LC 1, 59.3 years, is re-
439 garded as the reference fatigue life. It shows that the fatigue life decreases by 14.4 years,
440 or about 26%, when the scour depth is set as the maximum value of 1.3D without ap-
441 plying the TMD, compared to the reference fatigue life. When considering the time-
442 varying scour, the fatigue life decreases by about 22% from the reference value. When
443 comparing the results for LC 1 and LC 4, it shows the installation of the TMD results
444 in a significant increase in the fatigue life of the OWT, with an increase in fatigue life
445 of about 34.6 years, which about 62%. In LCs with the TMD installed, the fatigue life
446 in LC 6 decreases by about 18% when the scour depth reaches 1.3 D, compared to the



447 result in LC 4. But the fatigue life in LC 6 is still 1.25 times of the reference fatigue life,
 448 which indicates that the imposition of TMD can effectively increase the fatigue life of
 449 the OWT by reducing vibration amplitudes.

450



451 Fig. 10. Fatigue life of the wind turbine under six operating conditions

452 **4.5 Fatigue calculation with optimized TMD**

453 To compare the optimization effect and speed up the optimal parameter search
 454 process, the mass ratio of TMD is first kept as 1%. Before the optimization, the param-
 455 eter ranges of the frequency ratio and damping ratio need to be defined. The optimal
 456 frequency of the TMD is usually close to the resonance frequency of the main structure,
 457 so the range of the frequency ratio was chosen to be from 0.8 to 1.1 for optimization.
 458 On the other hand, as the optimal damping ratio could vary in a relatively larger range,
 459 the range of the damping ratio for optimization was chosen to be from 1% to 30%. The
 460 optimization of the TMD was also conducted with the mass ratio not fixed. A range of
 461 the mass ratio from 0.01 to 0.1 was used to optimize the TMD so that the influence of
 462 the mass ratio can be evaluated.

463 Table 6. Optimization of TMD parameters

Optimiza- tion method	Mass ratio range	Time-var- ying scour	Optimal mass ratio	Optimal fre- quency ratio	Optimal damping ratio	Fatigue life (Year)
Initial	0.01	Use	0.01	0.99	0.061	74.6
FOT	0.01	Use	0.01	0.89	0.035	80.0
FOT	0.01-0.1	Use	0.094	0.94	0.136	121.8

464 The optimal parameters obtained by FOT as well as the predicted fatigue life are
 465 listed in Table 6. The fatigue life for LC 5 and the parameters of the initially designed



466 TMD are also shown in Table 6 for comparison. It shows that when the mass ratio is
467 fixed at 1%, the optimal frequency ratio is 0.89, the optimal damping ratio is 3.5%, and
468 the final fatigue life is 80 years. Compared to the fatigue life with initially optimized
469 TMD using the traditional method without considering scour, the fatigue life is in-
470 creased by 5.4 years or about 7.2%. It indicates that the design of the TMD considering
471 time-varying scour depth is more beneficial to minimize fatigue damages. When the
472 mass ratio range is taken from 1% to 10%, the optimal mass ratio of the TMD is 9.4%,
473 the frequency ratio is 0.94, the damping ratio is 8.2%, and the final fatigue life is 121.8
474 years. In this case, the fatigue life of the OWT is significantly increased mainly due to
475 the large mass ratio. However, in practice, it might be uneconomic to implement a TMD
476 with such a large mass ratio.

477 5 Conclusions

478 This study establishes a rapid numerical model which can consider the effect of
479 scour and installation of a TMD. The established model was used to investigate the
480 influence of scouring and the installed passive structural control device on the OWT's
481 natural frequencies and fatigue life. An optimization technique was also developed to
482 find optimal parameters of the TMD considering time-varying scour. It shows that the
483 vibration amplitude of the OWT can be effectively reduced by the TMD. Results show
484 the vibration amplitude of the tower top decreases by about 7%. On the other hand,
485 when the scour depth reaches 1.3D, the wind turbine support structure becomes more
486 flexible, with the displacement of the tower top increased by about 8% without TMD.

487 In addition, the fatigue calculation results show that installation of the TMD sig-
488 nificantly extends the fatigue life of the OWT, but scour can cause a reduced perfor-
489 mance of the TMD. It is found that when the initially designed TMD does consider
490 scour and the scour-induced natural frequency reduction during the OWT's lifetime, its
491 performance is not as good as the TMD optimized by the developed FOT in terms of
492 fatigue life enhancement. Given a mass ratio of 1%, the fatigue life can be extended by
493 7.2% with the TMD optimized by FOT. This is because FOT can consider the effect of
494 time-varying scour. This study only performs the analysis with scour, but other factors
495 such as soil degradation can also alter the dynamic characteristics of OWTs and thus
496 have some influence on structural control devices' performance and fatigue life evalu-
497 ation. Additionally, during OWTs' lifetime, the properties of installed TMDs can also



498 change, making the evaluation of TMDs' performance and OWTs' fatigue life more
499 complicated. These factors are worthwhile investigating in the future.

500 6 **Competing interests**

501 The contact author has declared that none of the authors has any competing inter-
502 ests.

503 7 **Acknowledgements**

504 The financial supports from the National Natural Science Foundation of China (No.
505 52108280), Yangjiang Offshore Wind Laboratory (No. YJOWP-OF-2022A10),
506 the National Science Fund for Distinguished Young Scholars (No. 52025082) are
507 greatly appreciated.

508

509

510

511

512

513



514 **References**

- 515 Bergua, R., Robertson, A., Jonkman, J. and Platt, A. (2021). Specification Document
516 for OC6 Phase II: Verification of an Advanced Soil-Structure Interaction Model
517 for Offshore Wind Turbines (NREL/TP--5000-79938; p. NREL/TP--5000-
518 79938).
- 519 Bergua, R., Robertson, A., Jonkman, J., Platt, A., Page, A., Qvist, J., Amet, E., Cai, Z.,
520 Han, H., Beardsell, A., et al. (2022). OC6 Phase II: Integration and verification
521 of a new soil–structure interaction model for offshore wind design. *Wind En-
522 ergy*, 25, 793–810.
- 523 Branlard, E. (2017). *Wind Turbine Aerodynamics and Vorticity-Based Methods: Fun-
524 damentals and Recent Applications (Vol. 7)*. Cham: Springer International Pub-
525 lishing.
- 526 Chen, C. and Duffour, P. (2018). Modelling damping sources in monopile-supported
527 offshore wind turbines. *Wind Energy*, 21(11), 1121–1140.
528 <https://doi.org/10.1002/we.2218>
- 529 Chen, C., Duffour, P., Dai, K., Wang, Y. and Fromme, P. (2021). Identification of aer-
530 odynamic damping matrix for operating wind turbines. *Mech. Syst. Signal Pro-
531 cess.*, 154, 107568. <https://doi.org/10.1016/j.ymsp.2020.107568>
- 532 Chen, C., Duffour, P. and Fromme, P. (2020). Modelling wind turbine tower-rotor in-
533 teraction through an aerodynamic damping matrix. *J. Sound Vib.*, 489, 115667.
534 <https://doi.org/10.1016/j.jsv.2020.115667>
- 535 Chen, C., Duffour, P., Fromme, P. and Hua, X. (2021a). Numerically efficient fatigue
536 life prediction of offshore wind turbines using aerodynamic decoupling. *Renew.
537 Energy*, 178, 1421–1434. <https://doi.org/10.1016/j.renene.2021.06.115>
- 538 Chen, C., Duffour, P., Fromme, P. and Hua, X. (2021b). Numerically efficient fatigue
539 life prediction of offshore wind turbines using aerodynamic decoupling. *Renew.
540 Energy*, 178, 1421–1434. <https://doi.org/10.1016/j.renene.2021.06.115>
- 541 Chen, C., Duffour, P., Fromme, P., Shen, X., Hua, X. and Chen, Z. (2023). Simplified
542 complex-valued modal model for operating wind turbines through aerodynamic
543 decoupling and multi-blade coordinate transformation. *J. Sound Vib.*, 547,
544 117512. <https://doi.org/10.1016/j.jsv.2022.117512>
- 545 Chen, Y., Jin, X., Liu, H., Li, F. and Luo, M. (2021). Large scale wind turbine TMD
546 optimization based on Blade-Nacelle-Tower-Foundation Coupled Model.
547 *Ocean Eng.*, 239, 109764. <https://doi.org/10.1016/j.oceaneng.2021.109764>
- 548 Dai, K., Huang, H., Lu, Y., Meng, J., Mao, Z. and Camara, A. (2021). Effects of soil–
549 structure interaction on the design of tuned mass damper to control the seismic
550 response of wind turbine towers with gravity base. *Wind Energy*, 24(4), 323–
551 344. <https://doi.org/10.1002/we.2576>
- 552 Dai, S., Han, B., Wang, B., Luo, J. and He, B. (2021). Influence of soil scour on lateral
553 behavior of large-diameter offshore wind-turbine monopile and corresponding
554 scour monitoring method. *Ocean Eng.*, 239, 109809.
555 <https://doi.org/10.1016/j.oceaneng.2021.109809>
- 556 Den Hartog, J. P. (1957). *Mechanical Vibrations*. Fourth Edition. *Aeronaut. J.*, 61(554),
557 139–139.



- 558 Dinh, V.-N. and Basu, B. (2015). Passive control of floating offshore wind turbine nacelle and spar vibrations by multiple tuned mass dampers. *Struct. Control Health Monit.*, 22(1), 152–176. <https://doi.org/10.1002/stc.1666>
- 559
- 560
- 561 DNVGL-RP-0005. (2014a). RP-C203: Fatigue design of offshore steel structures.
- 562 DNV-OS-J101. (2014b). Design of Offshore Wind Turbine Structures.
- 563 Enevoldsen, I. and Mørk, K. J. (1996). Effects of a Vibration Mass Damper in a Wind Turbine Tower. *Mech. Struct. Mach.*, 24(2), 155–187. <https://doi.org/10.1080/08905459608905260>
- 564
- 565
- 566 Fard, M. M., Erken, A., Erkmen, B. and Ansal, A. (2022). Analysis of Offshore Wind Turbine by considering Soil-Pile-Structure Interaction: Effects of Foundation and Sea-Wave Properties. *J. Earthq. Eng.*, 26(14), 7222–7244. <https://doi.org/10.1080/13632469.2021.1961936>
- 567
- 568
- 569
- 570 Herbert, J. S. and Paul, S. V. (1994). Fatigue case study and reliability analyses for wind turbines. *Wind Energy Technol.*, 16, 950336.
- 571
- 572 IEC 61400-3-1. (2019). Wind energy generation systems Part 3-1: Design requirements for fixed offshore wind turbines.
- 573
- 574 Jonkman, B. J. and Buhl, M. L. (2006). TurbSim User’s Guide. Tech. Rep., 500, 39797.
- 575 Jonkman, J., Butterfield, S., Musial, W. and Scott, G. (2009). Definition of a 5-MW Reference Wind Turbine for Offshore System Development (NREL/TP-500-38060, 947422; p. NREL/TP-500-38060, 947422).
- 576
- 577
- 578 Jung, S., Kim, S.-R., patil, A. and Hung, L. C. (2015). Effect of monopile foundation modeling on the structural response of a 5-MW offshore wind turbine tower. *Ocean Eng.*, 109, 479–488.
- 579
- 580
- 581 Klaus, H., Dirk, J. O. and Peter, M. (1973). Measurements of wind-wave growth and swell decay during the joint North Sea wave project (JONSWAP).
- 582
- 583 Lackner, M. A. and Rotea, M. A. (2011). Passive structural control of offshore wind turbines. *Wind Energy*, 14(3), 373–388. <https://doi.org/10.1002/we.426>
- 584
- 585 Liang, F., Chen, H. and Jia, Y. (2018). Quasi-static p-y hysteresis loop for cyclic lateral response of pile foundations in offshore platforms. *Ocean Eng.*, 148, 62–74. <https://doi.org/10.1016/j.oceaneng.2017.11.024>
- 586
- 587
- 588 Ma, H. and Chen, C. (2021). Scour protection assessment of monopile foundation design for offshore wind turbines. *Ocean Eng.*, 231, 109083. <https://doi.org/10.1016/j.oceaneng.2021.109083>
- 589
- 590
- 591 Nakagawa, H. and Suzuki, K. (1976). Local Scour Around Bridge Pier in Tidal Current. *Coast. Eng. Jpn.*, 19(1), 89–100. <https://doi.org/10.1080/05785634.1976.11924219>
- 592
- 593
- 594 Peder Hyldal Sørensen, S. and Bo Ibsen, L. (2013). Assessment of foundation design for offshore monopiles unprotected against scour. *Ocean Eng.*, 63, 17–25. <https://doi.org/10.1016/j.oceaneng.2013.01.016>
- 595
- 596
- 597 Pedersen, D. M. and Askheim, H. (2021). Implementation of seismic soil-structure interaction in OpenFAST and application to a 10MW offshore wind turbine on jacket structure. Norwegian University.
- 598
- 599



- 600 Pelayo, F., Skaftø, A., Aenlle, M. L. and Brincker, R. (2015). Modal Analysis Based
601 Stress Estimation for Structural Elements Subjected to Operational Dynamic
602 Loadings. *Exp. Mech.*, 55(9), 1791–1802. <https://doi.org/10.1007/s11340-015-0073-6>
603
- 604 Prendergast, L. J., Gavin, K. and Doherty, P. (2015). An investigation into the effect of
605 scour on the natural frequency of an offshore wind turbine. *Ocean Eng.*, 101, 1–
606 11. <https://doi.org/10.1016/j.oceaneng.2015.04.017>
- 607 Rezaei, R. (2017). Fatigue Sensitivity of Monopile-supported Offshore Wind Turbines.
608 University College London.
- 609 Rezaei, R., Duffour, P. and Fromme, P. (2018). Scour influence on the fatigue life of
610 operational monopile-supported offshore wind turbines. *Wind Energy*, 21(9),
611 683–696. <https://doi.org/10.1002/we.2187>
- 612 Rudolph, D., Bos, K. J., Luijendijk, A. P. and Rietema, K. (2016). Scour around off-
613 shore structures-analysis of field measurements.
- 614 Shahmohammadi, A. and Shabakhty, N. (2020). Pile Apparent Fixity Length Estima-
615 tion for the Jacket-type Offshore Wind Turbines under Lateral Loads Applica-
616 ble to Fatigue Analysis. *Int. J. Coast. Offshore Eng.*, 3(4), 25–33.
617 <https://doi.org/10.29252/ijcoe.3.4.25>
- 618 Shirzadeh, R., Devriendt, C., Bidakhvidi, M. A. and Guillaume, P. (2013). Experi-
619 mental and computational damping estimation of an offshore wind turbine on a
620 monopile foundation. *J. Wind Eng. Ind. Aerodyn.*, 120, 96–106.
621 <https://doi.org/10.1016/j.jweia.2013.07.004>
- 622 Si, Y., Karimi, H. R. and Gao, H. (2013). Modeling and Parameter Analysis of the OC3-
623 Hywind Floating Wind Turbine with a Tuned Mass Damper in Nacelle. *J. Appl.*
624 *Math.*, 2013, 1–10. <https://doi.org/10.1155/2013/679071>
- 625 Sørensen, J. D., Frandsen, S. and Tarp-Johansen, N. J. (2008). Effective turbulence
626 models and fatigue reliability in wind farms. *Probabilistic Eng. Mech.*, 23(4),
627 531–538. <https://doi.org/10.1016/j.probengmech.2008.01.009>
- 628 Tempel, J. van der. (2006). Design of support structures for offshore wind turbines.
629 Technische Universiteit Delft.
- 630 Velarde, J., Kramhøft, C., Sørensen, J. D. and Zorzi, G. (2020). Fatigue reliability of
631 large monopiles for offshore wind turbines. *Int. J. Fatigue*, 134, 105487.
632 <https://doi.org/10.1016/j.ijfatigue.2020.105487>
- 633 Wang, L., Zhou, W., Guo, Z. and Rui, S. (2020). Frequency change and accumulated
634 inclination of offshore wind turbine jacket structure with piles in sand under
635 cyclic loadings. *Ocean Eng.*, 217, 108045.
636 <https://doi.org/10.1016/j.oceaneng.2020.108045>
- 637 Wang, X., Zeng, X., Li, X. and Li, J. (2019). Investigation on offshore wind turbine
638 with an innovative hybrid monopile foundation: An experimental based study.
639 *Renew. Energy*, 132, 129–141. <https://doi.org/10.1016/j.renene.2018.07.127>
- 640 Zdravković, L., Taborda, D., Potts, D., Jardine, R., Sideri, M., Schroeder, F., Byrne, B.,
641 McAdam, R., Burd, H., Houlsby, G., et al. (2015). Numerical modelling of large
642 diameter piles under lateral loading for offshore wind applications. *Front. Off-
643 shore Geotech.* III, 759–764.



- 644 Zhang, H., Liang, F. and Zheng, H. (2021). Dynamic impedance of monopiles for off-
645 shore wind turbines considering scour-hole dimensions. *Appl. Ocean Res.*, 107,
646 102493. <https://doi.org/10.1016/j.apor.2020.102493>
- 647 Zhang, R., Zhao, Z. and Dai, K. (2019). Seismic response mitigation of a wind turbine
648 tower using a tuned parallel inerter mass system. *Eng. Struct.*, 180, 29–39.
649 <https://doi.org/10.1016/j.engstruct.2018.11.020>
- 650
651